Soft Matter

ROYAL SOCIETY OF CHEMISTRY

PAPER

View Article Online
View Journal | View Issue

Check for updates

Cite this: *Soft Matter*, 2020, **16**, 3769

Hybrid granular hydrogels: combining composites and microgels for extended ranges of material properties†

Céline Samira Wyss, [a] Peyman Karami, [b] Pierre-Etienne Bourban *[a] and Dominique P. Pioletti *[b]

Received 6th February 2020,
Accepted 25th March 2020

DOI: 10.1039/d0sm00213e

rsc.li/soft-matter-journal

Developing hydrogels with optimal properties for specific applications is challenging as most of these properties, such as toughness, stiffness, swelling or deformability, are interrelated. The improvement of one property usually comes at the cost of another. In order to decouple the interdependence between these properties and to extend the range of material properties for hydrogels, we propose a strategy that combines composite and microgel approaches. The study focuses first on tailoring the swelling performance of hydrogels while minimally affecting other properties. The underlying principle is to partially substitute some of the hydrogels with pre-swollen microgels composed of the same materials. Swelling reductions up to 45% were obtained. Those granular hydrogels were then reinforced with nano-fibrillated cellulose fibres obtaining hybrid granular materials to improve their toughness and to further reduce their initial swelling. Four different structures of neat, granular and composite hydrogels including 63 different hydrogel compositions based on 20 kDa poly(ethylene glycol)dimethacrylate showed that the swelling ratio could be tailored without significantly affecting elastic modulus and deformation performance. The results explain the role of the PEGDM precursors on the swelling of the microgels as well as the influence of the microgel and fibre contents on the final properties. Moreover, the precursors of hydrogels with similar mechanical or swelling performance were injectable with a wide range of complex viscosities from 0.1 Pa s to over 1000 Pa s offering new opportunities for applications in confined as well as in unconfined environments.

1 Introduction

Hydrogels are known for their high water content, high biocompatibility, superabsorbent properties and relatively poor mechanical properties.[1–4] Those characteristics are suitable for a wide range of biomedical applications, such as tissue engineering,[5,6] tissue repair[7,8] or drug delivery[9,10] but also for soft robotics[11–13] or sensing applications.[14,15] Nevertheless, developing hydrogels with optimal properties is challenging as most of these properties, such as toughness, stiffness, fatigue resistance, swelling or processing ease, are interrelated. The improvement of one property usually comes at the cost of another as observed in many hydrogel structures including neat, double network or composite hydrogels.[16–21]

Granular hydrogels have gained a lot of attention recently. Their particular microstructure composed of contacting microgels offers an extended range of material properties for biomedical applications[22–29] or 3D printing.[27–29] Indeed, their precursor, only composed of microgels, is injectable and creates open microporosity between the microgels, which is ideal to transport nutriments or cells. To our knowledge this unique combination of properties was not achieved with other hydrogel structures. Moreover, they can be tailored in composition to explore additional biological, physical and mechanical properties.[23] For example, the group of L. De Laporte was able to guide and align cells growths by magnetically orienting rod-shape microgels *in situ* before curing the surrounding hydrogel. Moreover, the microgels were functionalized for being cell-adhesive or bioinert.[30]

Another challenge in hydrogel development is to better control the swelling performance while minimally affecting others properties, such as stiffness or deformation performance. Indeed, swelling of hydrogels might be critical in many medical,[31–33] food packaging[34] and soft robotic applications.[11–13] Different strategies have been investigated to tailor swelling. Changing the crosslinking type, crosslinking density, the polymer content, the polymer chain

[a] *Laboratory for Processing of Advanced Composites (LPAC), Ecole Polytechnique Fédérale de Lausanne (EPFL), CH-1015, Lausanne, Switzerland*
E-mail: pierre-etienne.bourban@epfl.ch
[b] *Laboratory of Biomechanical Orthopedics (LBO), Ecole Polytechnique Fédérale de Lausanne (EPFL), CH-1015, Lausanne, Switzerland*

† Electronic supplementary information (ESI) available. See DOI: 10.1039/d0sm00213e

length or the hydrophilicity of the polymer are commonly used methods. These approaches are efficient but often at the expense of other properties such as biocompatibility, stiffness, toughness or processability.[35–37] Recent methods employ cross-linking centres in the hydrogel, such as functionalized core–shell microgels or self-assembled micelles to bridge the polymer chains.[31,38,39] For example, Zhang *et al.* reported that their micelle-crosslinked hyaluronate hydrogel could be compressed up to 75% applied strain with an elastic modulus of 310 kPa and a swelling ratio of 9% only.[39] Alternatively, swelling can be controlled by influencing the maximum strand extension of the polymer chain such by incorporating rigid particles or fibres.[40] Moreover, apart from improved mechanical properties, the addition of reinforcement increases the dissipation mechanisms such as friction with the matrix or chemical interactions.[40–43]

Here we explore a new strategy by combining granular and composite hydrogels. In order to easily control swelling of hydrogels, part of the neat hydrogel (Fig. 1c) was substituted by pre-swollen microgels composed of the same material. Those hydrogels are defined as granular hydrogels (Fig. 1d). Thus, once immersed in water, mainly the surrounding matrix would swell. The second approach is to incorporate nanofibrillated cellulose (NFC) fibres in the hydrogels to obtain hydrogel composites (Fig. 1e) with improved toughness and reduced swelling.[21,44,45] Finally, hybrid granular hydrogels (Fig. 1f) combines granular and composite hydrogels. In order to understand the effect of the microgel and fibre contents on the processing ease, swelling and mechanical behaviour of the four different structures, 63 different hydrogel compositions based on 20 kDa poly(ethylene glycol)dimethacrylate (PEGDM) were studied.

2 Experimental

2.1 Materials

20 kDa poly(ethylene glycol)dimethacrylate (PEGDM) was purchased from Polysciences (ref. 25406-25, Germany). Nanofibrillated cellulose (NFC) from bleached softwood pulp were provide by Weidmann (WMFC-Standard). The length of most fibres varies between 50–500 μm, while their diameters between 0.1–10 μm. 20 kDa poly(ethylene glycol) (CAS 25322-68-3), mineral oil (CAS 8042-47-5) and span 80 (CAS 1338-43-8) were supplied by Merck. Irgacure 2959 from BASF was used as photoinitiator.

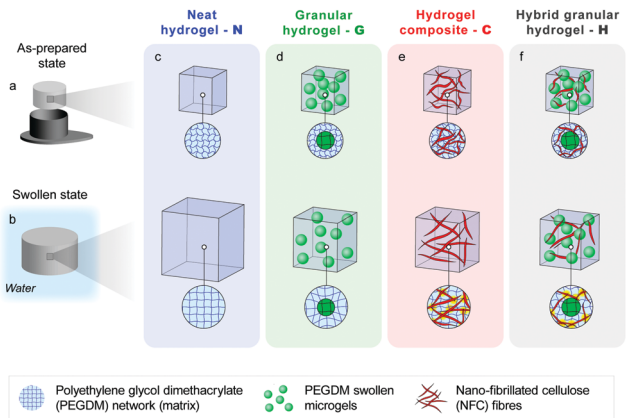

Fig. 1 Swelling behaviour from (a) the as-prepared state to (b) the fully swollen state of four different hydrogel structures: (c) neat hydrogel, (d) granular hydrogel, (e) hydrogel composite and (f) hybrid granular hydrogel.

2.2 Synthesis of hydrogels

The synthesis of microgels, initially composed of 10 wt% PEGDM are described in Fig. S1 in the ESI.† The particle size distribution of microgels were measured with a digital particle size analyser (Saturn DigiSizer II, micromeritics), where the refractive index was estimated at 1.334 with tomographic microscope (3D Nanolive Cell Explorer) and the density at 1.01 g cm^{-3}. As shown on Fig. S2 (ESI†) the size of particles varied from 20–160 μm.

The precursor of neat hydrogels was composed of 7–11 wt% of PEGDM, 0.1 g ml^{-1} % of Irgacure 2959 and distilled water. The precursor of hydrogel composites had the same PEGDM concentration than neat hydrogel, where 0.1–0.5 vol% NFC were added and mixed with an Ultra Turrax (IKA T25 digital, SN 25 10G) at 12 000 rps for 10 min. Granular hydrogels had similar composition as neat hydrogels but their precursors contained pre-swollen microgels composed of the same materials. Therefore, 3–6 wt% of dried microgels were pre-swollen in PEGDM precursor of different concentration, 2–7 wt%, in order to get a total PEGDM amount between 7–11 wt%. Note that the total PEGDM amount is the addition of the weight of dried PEGDM microgels with the PEGDM added in the precursor. Finally, the precursor of hybrid granular hydrogels had the similar composition than granular hydrogels were 0.1–0.5 vol% of NFC fibres were added. The precursors, degassed at 20 mbar, were casted in Eppendorf cup (∅ 5.3 mm × 3 mm) and covered with a microscopic glass before being irradiated for 30 min under UV-light irradiation at a wavelength of 365 nm and an intensity of 5 mW cm^{-2}. The gel fraction value of neat hydrogels – 10 wt% PEGDM was previously measured to be around 94%.[35]

2.3 Swelling ratios

The volume of the samples was determined with Archimedes' principle. The samples were immerged in extra pure hexane (99+%, Fisher Chemical) with a density of ρ = 0.659 g l^{-1}. In order to reach the equilibrium swelling state, the hydrogels were immersed in distilled water for at least 24 h before measuring the swelling ratio (SR) as following:

$$SR\ (vol\%) = 100 \times (V_{swollen} - V_{as\text{-}prepared})/V_{as\text{-}prepared} \quad (1)$$

where $V_{as\text{-}prepared}$ and $V_{swollen}$ correspond to the volume in the as-prepared and swollen state respectively. The average swelling ratios and their corresponding standard deviation errors were based on three different samples.

2.4 Mechanical properties

Cyclic compression loadings were performed as previously described[21] on swollen hydrogels with a tensile machine (5 kN Zwicky equipped with a 100 N load cell, Zwick Roell, Germany) at a constant displacement rate of 1 mm s^{-1}. In order to evaluate the real stress, it was considered that no change of volume occurs during loading time. Three samples were tested in swollen state under cyclic loading–unloading compression loading. They were five different stages during the tests:

- Stage 1: 3 cycles between 0% and 30% applied strain
- Stage 2: 3 cycles between 0% and 50% applied strain
- Stage 3: 3 cycles between 0% and 70% applied strain
- Stage 4: 3 cycles between 0% and 90% applied strain
- Stage 5: loading up to rupture if the samples could sustain deformation up to 90%

Representative loading curves of the four structures can be found in Fig. S3 in the ESI.† The elastic moduli were then determined by linear regression between 10% and 15% applied strain during the first loading cycle.

2.5 Microstructures

The morphology and distribution of the NFC fibres were observed in swollen hydrogels with an invert fluorescent confocal microscope (Zeiss LSM 700) equipped with a 20× lens and a laser of 405 nm. To enhance the fluorescence of NFC fibres, hydrogel composites and hybrid granular hydrogels were

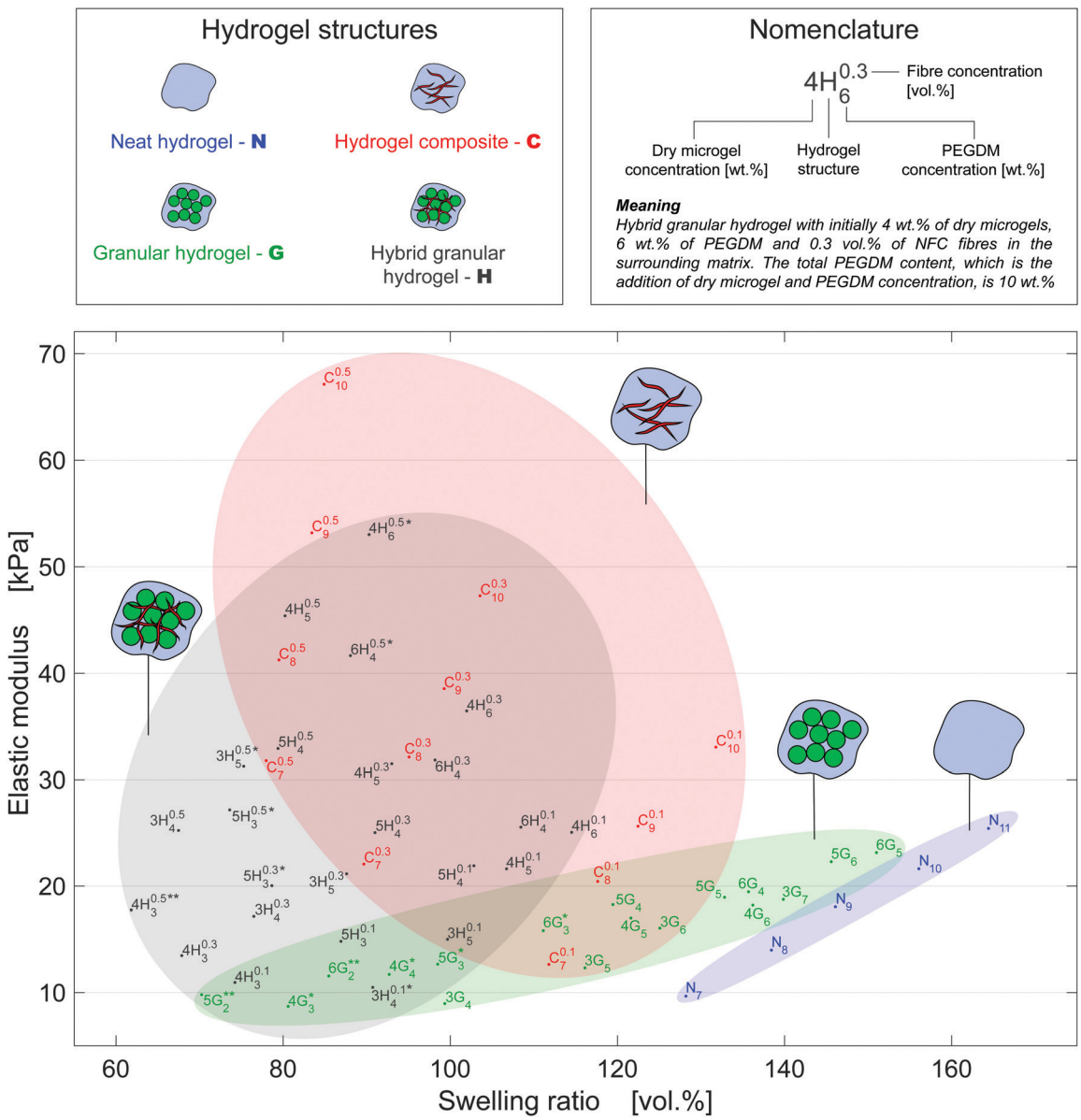

Fig. 2 Property chart of four different hydrogel structures with various compositions showing the elastic modulus determined between 10% and 15% applied strain in compression as a function of the swelling ratio measured with Archimedes' principle with (eqn 1). Most of the samples could resist more than 85% applied strain, those denoted with "*" broke between 80–85% applied strain and with "**" between 60–80% applied strain.

placed for at least 3 hours in 0.2 g l^{-1} Calcofluor White stain (Sigma-Aldrich, Buchs, CH) and 4 vol% of 10 wt% potassium hydroxide.

The surface of rupture and the microgels in freeze-dried hydrogels were observed with scanning electron microscopy (Zeiss Gemini) at 3.00 kV.

The surface profile of swollen broken hybrid granular hydrogels were imaged with 3D laser scanning microscope (VK-X200 Keyence) with a 20× lens.

2.6 Rheology

The complex viscosity of hydrogel precursors was evaluated at room temperature with a parallel plate rheometer (TA Instruments AR2000ex). An oscillating strain sweep at 0.5 Hz was then applied to the precursors, where the strain starts from 0.1% to 1000%.

3 Results & discussion

3.1 Swelling and mechanical properties

The swelling behaviour and mechanical performance of neat hydrogels, hydrogel composites, granular and hybrid granular hydrogels presented in Fig. 1, were measured and are shown on a property chart in Fig. 2. All presented data can be found in the Table S1 (ESI†). Note that the fibres were not incorporated in the microgels because the length of a few hundred micrometers of most fibres exceeded the size of the microgels, between 20–160 μm. Thus, the composition of microgels was kept the same for all granular compositions at 10 wt% PEGDM in the as-prepared state. Since the initial composition of microgels was the same as the one of the neat hydrogel N_{10}, their mechanical properties are expected to be similar.

Although 20 kDa PEGDM formed the bulk hydrogels of all structures, each structure covered a distinguishable zone as seen in Fig. 2. Neat hydrogels had the largest swelling ratio for similar elastic modulus. Both swelling ratio and elastic modulus increased with the PEGDM content. For a given elastic modulus, granular hydrogels had lower swelling ratio than neat hydrogels, especially below 15 kPa. As known previously,[21,44] the addition of fibres to neat hydrogels reduced swelling and increased the elastic modulus. This effect was promoted with increasing fibre content from 0.1 to 0.5 vol% NFC. A similar behaviour was observed for the hybrid granular hydrogels.

The loading curves of all hydrogels reinforced with NFC fibres, being the hydrogel composites and the hybrid granular hydrogels, had similar characteristics to the Mullins effect.

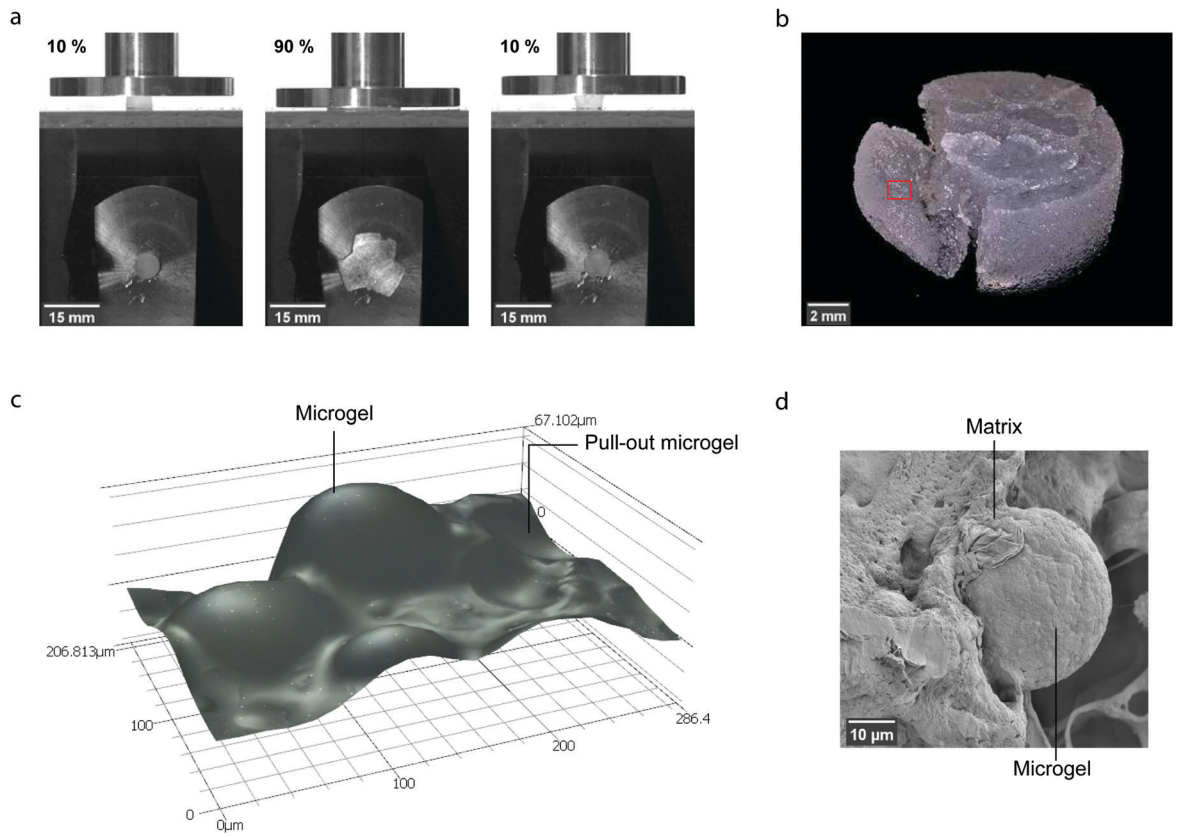

Fig. 3 Deformation to rupture of a representative broken hybrid granular hydrogel and the failure mechanisms at the surface of rupture. (a) Cyclic compression before, during and after 90% applied strain. The cross-section was visualized with a mirror at 45° under a transparent support. (b) Image taken with a digital microscope showing the sample $5H_3^{9.5}$ that broke at around 83% applied strain in compression. (c) Representative surface profile of a swollen sample highlighted with a red square in (b) showing how a crack had surrounded microgels during its propagation. (d) SEM images showing the interfacial decohesion between a microgel and the surrounding matrix.

As shown in Fig. S3 (ESI†), the hydrogel became softer after the first loading cycle. This behaviour was previously related to a local rearrangement of the fibre network.[44] Most samples could resist more than 85% applied strain. Some compositions of granular hydrogels denoted with "**" in Fig. 2 broke at lower strain, especially structures with low PEGDM concentrations in the surrounding matrix. Surprisingly, also some hybrid granular hydrogels showed some weakening at a higher cellulose concentration, 0.5 vol%, probably because of a lower fibre dispersion and formation of aggregates. Fig. 3 presents such a broken hybrid granular hydrogel and its surface of rupture. Interestingly, broken granular and composite structures could almost recover their original shape as shown in Fig. 3a and still sustain compression loading up to 98% applied strain. The rupture surface profile of a swollen hybrid granular hydrogel presented in Fig. 3b and c indicates that the crack surrounded and pulled-out microgels during its propagation. This means that the tough microgels did not break and that the interface between the microgels and the matrix was weaker than the bulk hydrogels. The occurrence of such interfacial decohesions is known to increase the toughness in composite materials.[46]

3.2 Effect of pre-swollen PEGDM microgels

The swelling behaviour of neat and granular hydrogels is presented in Fig. 4. As previously observed, granular hydrogels had lower swelling ratios as neat hydrogels. In order to better analyse the difference, the reduction of swelling was defined as following:

$$\text{Swelling reduction (\%)} = 100 \times (\text{SR}_{\text{N}_x} - \text{SR}_{y\text{G}_z})/\text{SR}_{\text{N}_x} \quad (2)$$

where "G" and "N" stand for granular and neat hydrogels respectively. The sum of the dry microgel content "y" and PEGDM contained in the surrounding matrix "z" is equal to the PEGDM content "x" of neat hydrogel. For example, the swelling ratio of granular hydrogel – $3G_4$ was compared with the one of neat hydrogel – N_7. Note that the error bars were calculated based on the rules of error propagation from the standard errors of the swelling ratios.

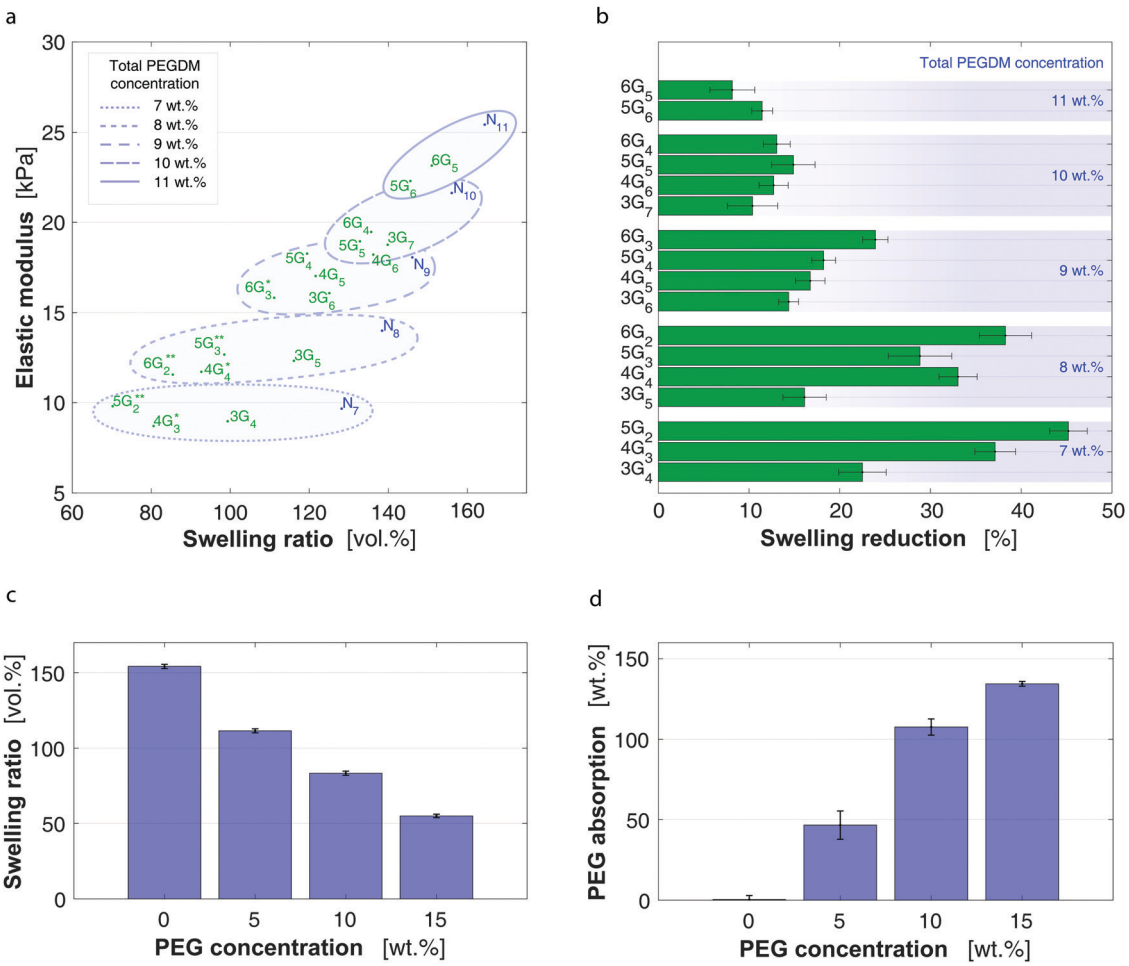

Fig. 4 Swelling behaviour of granular hydrogels: (a) property chart presenting the compressive elastic modulus *vs.* the swelling ratio obtained with eqn (1), (b) swelling reduction evaluated with eqn (2), where the total PEGDM content is the addition of dry microgel and PEGDM concentration. Influence of the PEG concentration of the immersion solutions on (c) the swelling ratio of the neat hydrogel N_{10} and (d) on the PEG absorption in the neat hydrogel N_{10} determined with eqn (3).

Fig. 4b shows that substituting neat hydrogels with pre-swollen microgels could reduce swelling by up to 45 ± 2%. Furthermore, the reduction of swelling was more efficient at lower total PEGDM concentrations, at higher microgel content and at lower PEGDM concentrations in the matrix. The smallest reduction of about 10% was measured for 11 wt% of total PEGDM content, where granular hydrogels and neat hydrogels presented similar swelling ratios of 160%. The elastic moduli increased proportionately with the total PEGDM amount. Unlike the swelling reduction, the elastic modulus depended on the material composition rather than on the microscopic structure of the hydrogel.

To better understand the swelling behaviour of granular hydrogels, the pre-swelling of microgels in the matrix precursor was investigated (see Movie S1 in the ESI†). Hydrogels of the same initial composition of microgels, 10 wt% PEGDM, were first dried before being swollen in different water/20 kDa polyethylene glycol (PEG) solutions. As shown in Fig. 4c, the swelling ratio, obtained with eqn (1), significantly decreased with increasing PEG concentration, probably due to the osmotic pressure induced by PEG.[47] This suggests that microgels pre-swell less in precursors of higher PEGDM concentrations. Thus, once polymerized and immersed in water, those granular hydrogels would swell more because the microgels were not fully swollen. In other words, higher pre-swelling levels of microgels induced by lower PEGDM concentrations in the matrix will better reduce swelling. For the hydrogels evaluated in this study, it is expected that above 11 wt% of total PEGDM, the reduction of swelling becomes negligible.

In order to estimate if PEGDM diffuses from the precursors into the microgels, three neat hydrogels N_{10} with the same initial composition as the microgels were first dried and weighed (m_{dry}) before being swollen in different PEG solutions. Then the hydrogels were retrieved from the solutions, dried and weighed (m_{PEG_dry}) again. The PEG absorption (PEG_{abs}) was estimated as following:

$$PEG_{abs}\ (wt\%) = 100 \times (m_{dry} - m_{PEG\_dry})/m_{dry} \qquad (3)$$

As shown in Fig. 4d, the PEG absorption increased with the PEG concentration in the hydrating solution. Similarly, PEGDM

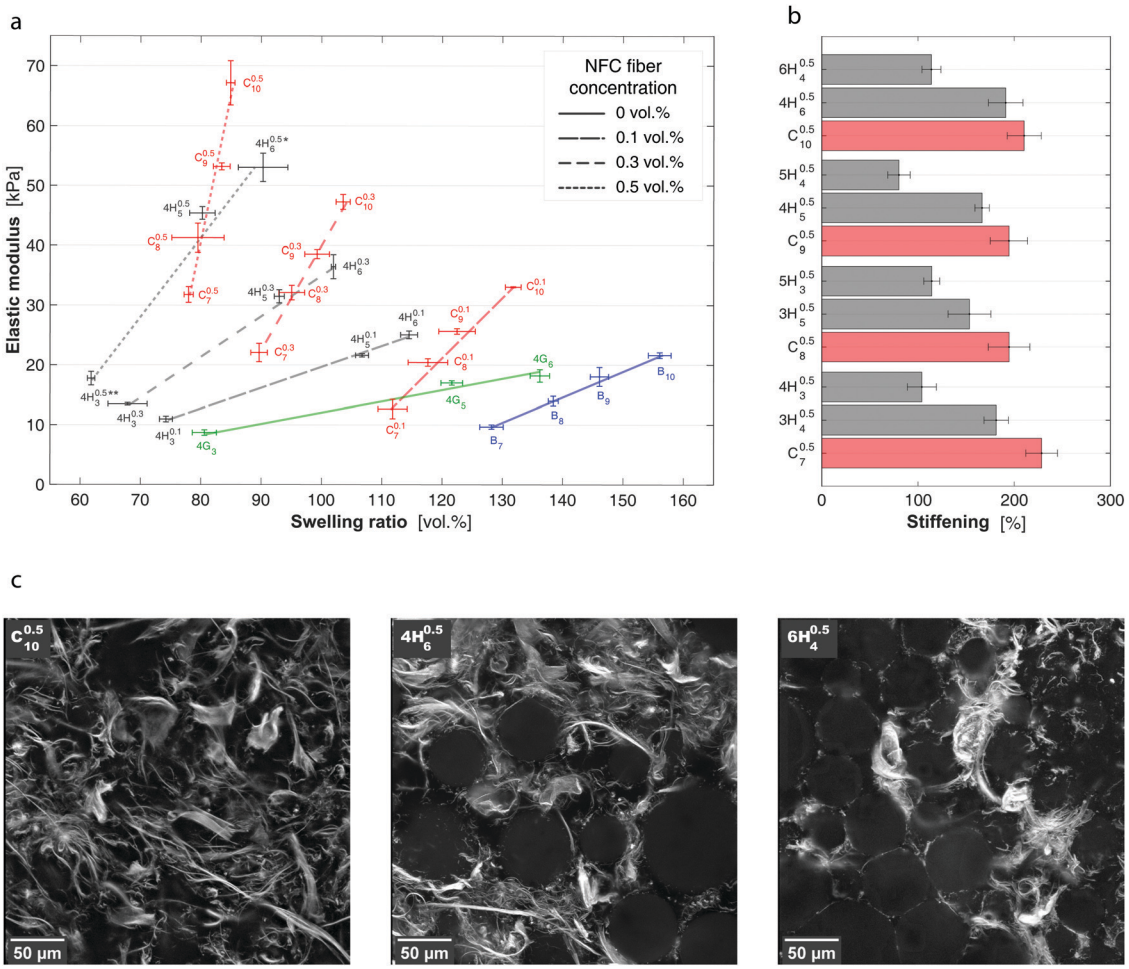

Fig. 5 Effect of NFC fibre concentration. (a) Property chart presenting the compressive elastic modulus *vs.* the swelling ratio. The effect of the fibres concentration is highlighted with linear fits. (b) Stiffening achieved when 0.5 vol% of NFC fibres are added to the analogous hydrogel, calculated with eqn (4) and (5). (c) Z-stack projection of 7.5 µm in depth taken with a fluorescent confocal microscope showing the NFC fibres and microgels incorporated in swollen hydrogels.

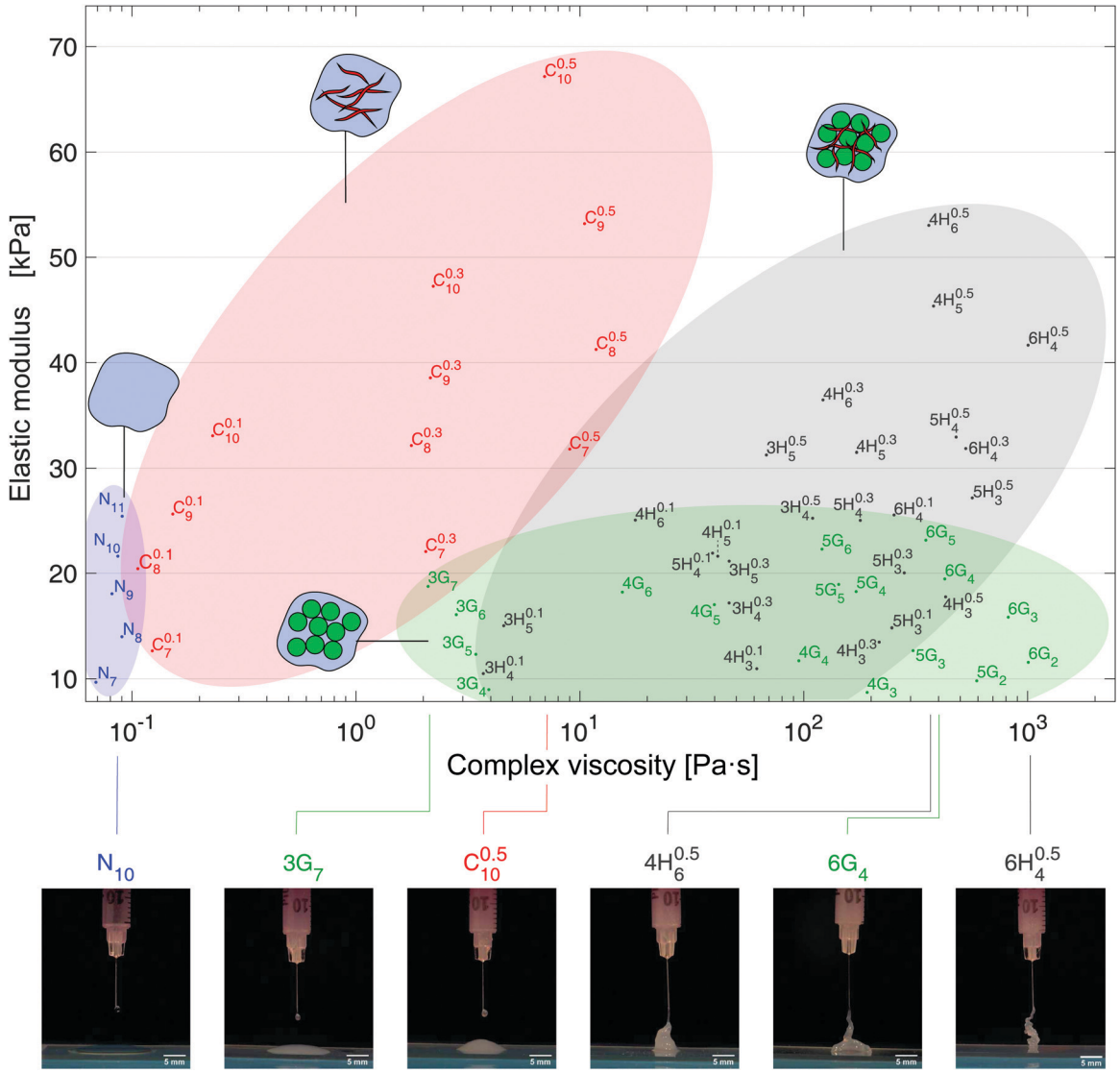

Fig. 6 Property chart of four different hydrogel structures with various composition showing the elastic modulus in compression as a function of the complex viscosity of the precursors at 0.1% oscillation strain and 0.5 Hz. Although a wide range of complex viscosity could be achieved, all precursors were injectable through a needle with an inner diameter of 0.133 mm.

from the precursor is expected to diffuse into the microgels, which would strengthen the interface between microgels and the matrix and homogenise the PEGDM concentration in the granular hydrogels. Nevertheless, the variations in swelling and in local PEGDM concentrations makes it difficult to estimate the precise volume occupied by microgels in granular hydrogels. Moreover, for better assessing the swelling behaviour of microgels, monodisperse distribution would be required in order to consider the effective role of their surface to volume ratio.[48] Indeed, measuring swelling by statistical methods would be easier than tracking individual microgels.

3.3 Effect of cellulose fibres

Fig. 5 presents the effect of incorporating NFC fibres in neat hydrogels (hydrogel composites) and in the matrix of the granular hydrogels (hybrid granular hydrogels). As observed in Fig. 2, adding fibres increased the elastic moduli and reduced the swelling ratios of both structures. Highlighted with a steeper linear regression in Fig. 5a, the effect of fibres was getting stronger with increasing the fibre concentration from 0.1 to 0.5 vol% NFC and started to dominate the effect of the total PEGDM content.

Fig. 5b reports the different stiffening achieved when 0.5 vol% NFC fibres were added to the analogous neat hydrogel in red and granular hydrogel in grey. The stiffening was calculated as described in eqn (4) for conventional structures and eqn (5) for granular structures.

$$\text{Stiffening } (\%) = 100 \times \left(E_{C_x^{0.5}} - E_{N_x}\right) \Big/ E_{N_x} \qquad (4)$$

where "N" and "C" are the abbreviations of neat hydrogel and hydrogel composite respectively and "x" for the PEGDM

concentration.

$$\text{Stiffening}\ (\%) = 100 \times \left(E_{yH_x^{0.5}} - E_{yG_x}\right) \Big/ E_{yG_x} \qquad (5)$$

where "H" and "G" stand for granular and hybrid granular hydrogels, "*y*" for the dry microgel content and "*x*" for the PEGDM contained in the surrounding matrix. For example, the elastic modulus of the hydrogel composite C_{10} was compared with the one of the neat hydrogel N_{10} and reached a 200% stiffening. Note that the error bars were calculated based on the rules of error propagation from the standard errors of the elastic moduli.

While the stiffening of 200% achieved by the hydrogel composites seemed not being affected by the total PEGDM amount, the granular structures showed more variations. In particular, the stiffening was reduced from around 200% to 80% at higher microgel concentrations and lower PEGDM contents in the surrounding matrix.

In order to understand the stiffening behaviour, the fibre distribution in swollen hydrogel composites and hybrid hydrogels were observed under a fluorescent confocal microscope. Fig. 5c shows z-stack projections of swollen hydrogels containing initially a total PEGDM concentration of 10 wt% PEGDM and 0.5 vol% NFC fibres. The fibres in the hydrogel composite ($C_{10}^{0.5}$) were better dispersed compared to hybrid granular hydrogels ($4H_6^{0.5}$, $6H_4^{0.5}$). Indeed, the presence of local fibre concentration and the formation of aggregates increased with the microgel concentration. Both affected the stiffening efficiency and the deformability of hybrid granular hydrogels.

4 Processing

The processing ease of the developed hydrogel structures for different applications depends on the processability of the hydrogel precursors. Therefore, their rheological behaviour was studied with a parallel plate rheometer at 0.5 Hz and oscillating strains going from 0.1% to 1000%. The range of complex viscosities observed at quasi static 0.1% strain of different hydrogel precursors are presented in Fig. 6. The complex viscosities at larger strain levels are reported in the Table S1 (ESI†).

Neat hydrogel precursors had a very low complex viscosity, less than 0.1 Pa s. At 0.1% strain, the complex viscosity of hydrogel composite precursors increased from 0.1 to 10 Pa s with the fibre concentrations. Both precursors would still be convenient to be injected through narrow needles (Movies S2 and S3 in the ESI†). The complex viscosities of the precursors of granular and hybrid granular hydrogels varied from 2 to 1000 Pa s and could thus be up to 10 000 times more viscous as the one of neat hydrogel precursors (see Movies S4–S7, ESI†). Moreover, above 500 Pa s, the precursors started to behave similarly to jammed microgels as shown in Fig. 6 and in the Movie S7 in the ESI.† In addition, the complex viscosity decreased with increasing PEGDM concentration in the matrix precursor. In fact, PEGDM act as lubricant for the microgels. As already mentioned in the study on the swelling, at higher PEGDM concentrations in the precursor, the microgels occupy less volume and furthermore PEGDM reduces friction between the microgels. Moreover, all precursors of the hydrogel composites and hybrid granular hydrogels showed obvious shear-thinning behaviour after 10% strain as shown on Fig. S4 in the ESI.† This is a key advantage for the continuous placement of the materials before or during the crosslinking *via* 3D printing manufacturing.

In summary, depending on the hydrogel structure, a large range of precursor's complex viscosities could be obtained, while keeping similar mechanical properties of the hydrogels, which offers new applications opportunities. For example, low precursors' complex viscosity would be suitable for confined applications, such as the replacement of nucleus pulposus,[49] while precursors of high complex viscosity would be ideal for unconfined applications like the replacement of focal cartilage defects without the use of a membrane[50] or to 3D printed complex unconfined structures.[41]

5 Conclusions

A novel strategy was proposed to easily control swelling and stiffness of hydrogel materials by integrating microgels and fibres in order to obtain hybrid granular hydrogels with unique microscopic structures. An extensive assessment of different structures including 63 different hydrogel compositions based on PEGDM showed that the swelling ratio could be tailored from 60 vol% to 165 vol% without significantly losing stiffness and deformation. Reduction of swelling up to 45% was obtained by integrating pre-swollen microgel into neat hydrogels. The achievable swelling reduction of the final hydrogels is given by the microgels concentration and by the total PEGDM content of the microgels and of the matrix around them. The studied material system encountered a negligible swelling reduction at above 11 wt% of total PEGDM content, where granular hydrogels and their representative neat hydrogels had similar swelling ratios. The reason was related to the swelling degree of microgels that would pre-swell less in precursors of higher PEGDM concentrations.

For a given elastic modulus, granular hydrogels had lower swelling ratios than neat hydrogels, especially below 15 kPa. The addition of fibres reduced swelling and increased the elastic modulus of both, the hydrogel composites and the hybrid granular structures. The effect was getting stronger with increasing fibre content and started to be predominant above a fibre concentration of 0.3 vol% NFC. However, too high local concentrations of cellulose fibres confined in between the microgels could lead to earlier failure.

All precursors were injectable and the one incorporating microgels and/or cellulose fibres showed obvious shear-thinning behavior required for advanced 3D printing. This opens a new horizon for processing in confined as well as in unconfined environments and using these material systems when precise control of stiffness and minimum swelling is needed. Based on these first hybrid granular structures, the

integration of other types of hydrogels, microgels and fibres can be envisaged.

Conflicts of interest

There are no conflicts to declare.

Acknowledgements

The financial support is given by the Swiss National Science Foundation (grant CR 2312-137743). The help of Michael Kessler and Esther Amstad from the Soft Material Laboratory (SMaL) at EPFL is very much appreciated. Optics Platform (BIOP) and Interdisciplinary Centre for Electron Microscopy (CIME) at EPFL provided support for the microscopy.

References

1 F. Ganji, S. V. Faraahani and E. Vasheghani-Farahani, *Iran. Polym. J.*, 2010, **19**, 375–398.
2 A. S. Hoffman, *Adv. Drug Delivery Rev.*, 2012, **64**(Supp. l), 18–23.
3 M. Quesada-Pérez, J. Alberto Maroto-Centeno, J. Forcada and R. Hidalgo-Alvarez, *Soft Matter*, 2011, **7**, 10536–10547.
4 F. Ullah, M. B. H. Othman, F. Javed, Z. Ahmad and H. M. Akil, *Mater. Sci. Eng., C*, 2015, **57**, 414–433.
5 K. Y. Lee and D. J. Mooney, *Chem. Rev.*, 2001, **101**, 1869–1880.
6 A. Sivashanmugam, R. Arun Kumar, M. Vishnu Priya, S. V. Nair and R. Jayakumar, *Eur. Polym. J.*, 2015, **72**, 543–565.
7 A. M. S. Costa and J. F. Mano, *Eur. Polym. J.*, 2015, **72**, 344–364.
8 S. An, E. J. Jeon, J. Jeon and S.-W. Cho, *Mater. Horiz.*, 2019, **6**, 1169–1178.
9 J. Li and D. J. Mooney, *Nat. Rev. Mater.*, 2016, **1**, 16071.
10 G. He, S. Chen, Y. Xu, Z. Miao, Y. Ma, H. Qian, Y. Lu and Z. Zha, *Mater. Horiz.*, 2019, **6**, 711–716.
11 D. Han, C. Farino, C. Yang, T. Scott, D. Browe, W. Choi, J. W. Freeman and H. Lee, *ACS Appl. Mater. Interfaces*, 2018, **10**, 17512–17518.
12 W. J. Zheng, N. An, J. H. Yang, J. Zhou and Y. M. Chen, *ACS Appl. Mater. Interfaces*, 2015, **7**, 1758–1764.
13 L. Jing, K. Li, H. Yang and P.-Y. Chen, *Mater. Horiz.*, 2020, **7**, 54–70.
14 T. Hiratani, O. Kose, W. Y. Hamad and M. J. MacLachlan, *Mater. Horiz.*, 2018, **5**, 1076–1081.
15 D. Buenger, F. Topuz and J. Groll, *Prog. Polym. Sci.*, 2012, **37**, 1678–1719.
16 J. P. Gong, *Soft Matter*, 2010, **6**, 2583–2590.
17 E. S. Dragan, *Chem. Eng. J.*, 2014, **243**, 572–590.
18 R. E. Webber, C. Creton, H. R. Brown and J. P. Gong, *Macromolecules*, 2007, **40**, 2919–2927.
19 Q. Chen, X. Yan, L. Zhu, H. Chen, B. Jiang, D. Wei, L. Huang, J. Yang, B. Liu and J. Zheng, *Chem. Mater.*, 2016, **28**, 5710–5720.
20 P. Karami, C. S. Wyss, A. Khoushabi, A. Schmocker, M. Broome, C. Moser, P.-E. Bourban and D. P. Pioletti, *ACS Appl. Mater. Interfaces*, 2018, **10**, 38692–38699.
21 A. Khoushabi, C. S. Wyss, B. Caglar, D. Pioletti and P.-E. Bourban, *Compos. Sci. Technol.*, 2018, **168**, 88–95.
22 H. Du, A. Cont, M. Steinacher and E. Amstad, *Langmuir*, 2018, **34**, 3459–3466.
23 L. Riley, L. Schirmer and T. Segura, *Curr. Opin. Biotechnol.*, 2019, **60**, 1–8.
24 J. E. Mealy, J. J. Chung, H.-H. Jeong, D. Issadore, D. Lee, P. Atluri and J. A. Burdick, *Adv. Mater.*, 2018, **30**, 1705912.
25 M. H. Chen, J. J. Chung, J. E. Mealy, S. Zaman, E. C. Li, M. F. Arisi, P. Atluri and J. A. Burdick, *Macromol. Biosci.*, 2018, **0**, 1800248.
26 D. R. Griffin, W. M. Weaver, P. O. Scumpia, D. Di Carlo and T. Segura, *Nat. Mater.*, 2015, **14**, 737–744.
27 L. Moroni, J. A. Burdick, C. Highley, S. J. Lee, Y. Morimoto, S. Takeuchi and J. J. Yoo, *Nat. Rev. Mater.*, 2018, **3**, 21–37.
28 S. Xin, D. Chimene, J. E. Garza, A. K. Gaharwar and D. L. Alge, *Biomater. Sci.*, 2019, **7**, 1179–1187.
29 C. B. Highley, K. H. Song, A. C. Daly and J. A. Burdick, *Adv. Sci.*, 2018, 1801076.
30 J. C. Rose, D. B. Gehlen, T. Haraszti, J. Köhler, C. J. Licht and L. De Laporte, *Biomaterials*, 2018, **163**, 128–141.
31 P. Ren, H. Zhang, Z. Dai, F. Ren, Y. Wu, R. Hou, Y. Zhu and J. Fu, *J. Mater. Chem. B*, 2019, **7**, 5490–5501.
32 A. Schmocker, A. Khoushabi, D. A. Frauchiger, B. Gantenbein, C. Schizas, C. Moser, P.-E. Bourban and D. P. Pioletti, *Biomaterials*, 2016, **88**, 110–119.
33 R. Marcombe, S. Cai, W. Hong, X. Zhao, Y. Lapusta and Z. Suo, *Soft Matter*, 2010, **6**, 784–793.
34 R. A. Batista, P. J. P. Espitia, J. de, S. S. Quintans, M. M. Freitas, M. Â. Cerqueira, J. A. Teixeira and J. C. Cardoso, *Carbohydr. Polym.*, 2019, **205**, 106–116.
35 A. Khoushabi, A. Schmocker, D. P. Pioletti, C. Moser, C. Schizas, J. A. Månson and P. E. Bourban, *Compos. Sci. Technol.*, 2015, **119**, 93–99.
36 J. S. Temenoff, K. A. Athanasiou, R. G. LeBaron and A. G. Mikos, *J. Biomed. Mater. Res.*, 2002, **59**, 429–437.
37 E. O. Akala, P. Kopecková and J. Kopecek, *Biomaterials*, 1998, **19**, 1037–1047.
38 H. Wang, P. Li, K. Xu, Y. Tan, C. Lu, Y. Li, X. Liang and P. Wang, *Colloid Polym. Sci.*, 2016, **294**, 367–380.
39 H. Zhang, P. Ren, Y. Jin and F. Ren, *Mater. Lett.*, 2019, **243**, 112–115.
40 J. Djonlagić, D. Žugić and Z. Petrović, *J. Appl. Polym. Sci.*, 2012, **124**, 3024–3036.
41 A. M. S. Costa and J. F. Mano, *Chem. Commun.*, 2015, **51**, 15673–15676.
42 H.-P. Cong, P. Wang and S.-H. Yu, *Small*, 2014, **10**, 448–453.
43 M. Zhong, Y.-T. Liu and X.-M. Xie, *J. Mater. Chem. B*, 2015, **3**, 4001–4008.
44 C. S. Wyss, P. Karami, P.-E. Bourban and D. P. Pioletti, *Extreme Mech. Lett.*, 2018, **24**, 66–74.
45 A. Khoushabi, A. Schmocker, D. P. Pioletti, C. Moser, C. Schizas, J. A. Månson and P. E. Bourban, *Compos. Sci. Technol.*, 2015, **119**, 93–99.
46 F. Barthelat and R. Rabiei, *J. Mech. Phys. Solids*, 2011, **59**, 829–840.

47 S. Sohn, H. H. Strey and S. P. Gido, *Biomacromolecules*, 2004, **5**, 751–757.
48 A. A. Karanastasis, Y. Zhang, G. S. Kenath, M. D. Lessard, J. Bewersdorf and C. K. Ullal, *Mater. Horiz.*, 2018, **5**, 1130–1136.
49 A. Schmocker, A. Khoushabi, D. A. Frauchiger, B. Gantenbein, C. Schizas, C. Moser, P.-E. Bourban and D. P. Pioletti, *Biomaterials*, 2016, **88**, 110–119.
50 M. Falah, G. Nierenberg, M. Soudry, M. Hayden and G. Volpin, *Int. Orthop.*, 2010, **34**, 621–630.